PAPER • OPEN ACCESS

Manipulating 1-dimensional skyrmion motion by the external magnetic field gradient

New Journal of Physics
The open access journal at the forefront of physics

Deutsche Physikalische Gesellschaft DPG
IOP Institute of Physics

Published in partnership with: Deutsche Physikalische Gesellschaft and the Institute of Physics

OPEN ACCESS

RECEIVED
8 July 2020

REVISED
9 September 2020

ACCEPTED FOR PUBLICATION
6 October 2020

PUBLISHED
22 October 2020

PAPER

Manipulating 1-dimensional skyrmion motion by the external magnetic field gradient

Jaehun Cho[1,2,7,*], Eiiti Tamura[2,3,4,7], Chaozhe Liu[5], Soma Miki[2,3], Chun-Yeol You[6], June-Seo Kim[1], Hikaru Nomura[2,3,5], Minori Goto[2,3], Ryoichi Nakatani[5] and Yoshishige Suzuki[2,3,*]

[1] Division of Nanotechnology, Daegu Gyeongbuk Institute of Science and Technology (DGIST), Daegu, Republic of Korea
[2] Graduate School of Engineering Science, Osaka University, Toyonaka, Osaka, Japan
[3] Center for Spintronics Research Network, Osaka University, Toyonaka, Osaka, Japan
[4] Department of Electronic Science and Engineering, Kyoto University, Kyoto, Kyoto, Japan
[5] Graduate School of Engineering, Osaka University, Suita, Osaka, Japan
[6] Department of Emerging Materials Science, Daegu Gyeongbuk Institute of Science and Technology (DGIST), Daegu, Republic of Korea
[*] Authors to whom any correspondence should be addressed.
[7] These authors contributed equally to this work.

E-mail: jhcho@dgist.ac.kr and suzuki-y@mp.es.osaka-u.ac.jp

Keywords: skyrmion motion, micromagnetic simulations, skyrmions accelerated by a gradient of the external magnetic field

Abstract

We have investigated an approximated analytic form of the one-dimensional motion of skyrmions accelerated by a gradient of the external magnetic field. We find excellent agreement between the analytical calculations and micromagnetic simulations when the skyrmion size is large. The skyrmion motion is related to not only the skyrmion size but also the skyrmion wall width. We also have performed the numerical calculation without approximation in comparison. The numerical calculation results are entirely in agreement with those of micromagnetic simulation for all the skyrmion size. These results introduce an efficient control of skyrmions to next-generation spintronic devices.

1. Introduction

In magnetic heterojunction systems, the crucial competition among Heisenberg exchange interaction, Dzyaloshinskii–Moriya (DM) interaction, and magnetocrystalline anisotropy can exhibit complex spin textures such as Skyrmions [1, 2], chiral magnetic domain walls (DWs) [3–5], and Bloch lines [6, 7]. A contribution of interfacial DM interaction is directly related to the spin–orbit coupling at the interfaces between heavy metals and ferromagnets combined with the broken inversion symmetry at the interfaces [8–12]. These exotic spin textures arising from DM interaction are mostly topologically stable and are appropriate for various applications as an information carrier and information-processing devices [13, 14]. Indeed, a large majority of theoretical and numerical studies have shown the possibilities that magnetic skyrmions and chiral DWs could be essential ingredients of the next-generation spintronic devices for storage devices and logic application [8, 14]. A single or a bunch of these topological objects are manipulated by laterally applied electrical currents due to spin-transfer torque [15, 16] or spin–orbit torque [17, 18]. Below the critical current density, the magnetic textures are fastened in a pinning potential. When the electric current is larger than the critical current density, the non-negligible displacements of topological objects occur. While the electrical current injection technique is a promising method to drive multiple skyrmions and chiral DWs synchronously, a large critical current density caused by low resistivities of magnetic materials and the extremely narrow and long nanoscale wire architectures makes an insurmountable obstacle which is the so-called 'Joule heating problem' owing to Ohmic losses [19, 20].

Many studies of alternative propagation techniques have been carried out using not only to overcome the issue of the Joule heating problem but also application in skyrmions such as magnetic anisotropy

gradient [21], electric field gradient [22, 23], temperature gradient [24–26], spin waves and magnons [26–29]. At present, extensive experiments observed the skyrmion motion on the tracks with the magnetic anisotropy energy [30], controlled by external electric fields [31]. Moreover, there are several papers about the skyrmion motion under external magnetic field gradient [32–36]. Zhang *et al* [32] report that rotational motion under the radial field gradient. Casiraghi *et al* [33] reported experimental results that skyrmion manipulates individually through the local field gradient. Liang *et al* [34] demonstrate that the skyrmion motion under a magnetic field gradient at the limited region of damping. Komineas and Papanicolaou [35] report cyclotron-types rotational motion in the two-dimension. Wang *et al* [36] claim that radially spatial gradient magnetic field along the width direction on the nanowire. Utilizing magnetic anisotropy energy, electric fields, and gradient magnetic field, we have established ultra-low energy-consumption spintronics devices. The skyrmion tracks patterned with difference of the magnetic anisotropy energy, will be playing an important role to realize the Brownian computation [30].

The magnetic field-driven chiral DWs and magnetic solitons have been received a great amount of interests because the system is totally governed by the Landau–Lifshitz (LL) equation, which is equivalent to the Landau–Lifshitz–Gilbert (LLG) equation when the magnetic damping constant of the system is small enough. Moreover, various manipulation ideas such as direct current or alternative current magnetic field-driven magnetic solitons, the transverse magnetic field pulse induced DW, and skyrmion racetrack are demonstrated recently [37, 38]. For practical applications for information storage devices or logic applications, the magnetic skyrmion or DW racetrack should be compatible with the complementary metal–oxide–semiconductor (CMOS) architectures, and the continuous miniaturization of CMOS architectures is essential for increasing the data capacity of the devices. For the magnetic field-driven skyrmion or DW motions in real spintronic devices, the external magnetic field is applied from the ultrashort electrical current pulses passing through the conduction lines adjacent skyrmion or DW racetracks to minimize the energy consumptions. Naturally, the applied magnetic field to the magnetic racetracks is not uniform due to Oersted law.

In this work, we investigate analytically and computationally the skyrmion motion in a one-dimensional nanowire driven by the magnetic field along the z-direction while the field gradient is taken in the x-direction. According to the analytic formula, the skyrmion velocity in the nanowire with a magnetic field gradient is proportional to the skyrmion radius and the wall width. The analytic calculation is in good agreement with the micromagnetic simulation results when the skyrmion size is large. Furthermore, we also perform the numerical calculation without approximation in comparison. The numerical calculation results are entirely in agreement with those of micromagnetic simulation in a whole range of the skyrmion size. The observed results can be introduced to next-generation spintronics devices.

2. Analytical formula for the skyrmion velocity driven by the magnetic-field gradient

We briefly describe a theory for the skyrmion motion in our system. The motion of skyrmion in a two-dimensional film can be expressed by the Thiele equations [39]

$$\boldsymbol{G}\times\dot{\boldsymbol{R}}+\alpha\mathcal{D}\dot{\boldsymbol{R}}=\boldsymbol{F}, \tag{1}$$

where $\boldsymbol{R}$ is the center coordinate, $\boldsymbol{G}$ the gyromagnetic coupling, α the Gilbert damping constant, $\mathcal{D}$ the dissipation dyadic, and $\boldsymbol{F}$ the external force, e.g., by electric currents, magnetic field gradients, and thermal fluctuations.

The gyromagnetic coupling vector $\boldsymbol{G}=(0,0,-G)$ is given by, $G=\int_V \hat{g}_{ij}\ \mathrm{d}V=4\pi q\frac{M_s}{|\gamma|}$. Here, $\hat{g}_{ij}=\frac{M_s}{|\gamma|}\boldsymbol{m}\cdot\left(\frac{\partial\boldsymbol{m}}{\partial x_i}\times\frac{\partial\boldsymbol{m}}{\partial x_j}\right)$, M_s is the saturation magnetization, γ the gyromagnetic ratio. The normalized magnetization at $\boldsymbol{r}=(r,\phi)$ is described by polar and azimuthal angles $\Theta(r,\phi)$ and $\Phi(r,\phi)$ so that $\boldsymbol{m}=(\sin\Theta\cos\Phi,\ \sin\Theta\sin\Phi,\cos\Theta)$. A skyrmion centered at $r=0$ can be described [40] by,

$$\Theta=\Theta(r),\Phi=q\phi+\gamma, \tag{2}$$

with boundary conditions of $\Theta(0)=0$ and $\Theta(\infty)=\pi$ for the axial symmetric skyrmion. The integer q is the vorticity ($q=1$ for the skyrmion and $q=-1$ for an anti-skyrmion), and γ is the helicity classifying the type of skyrmions ($\gamma=0$ or π for Néel skyrmions and $\gamma=\pm\pi/2$ for Bloch skyrmions). For the Néel skyrmion, the magnetization profile looks like a 360° Néel domain wall along the radial direction as described below [41, 42]

$$\Theta(r)=2\ \arctan\left(\frac{\sinh\left(\left(\frac{r}{w}\right)\right)}{\left(\sinh\left(\frac{R}{w}\right)\right)}\right), \tag{3}$$

where R is the radius of the skyrmion, w the wall width of the skyrmion, and r the position of magnetization. The components of the dissipative force, which is the second term of equation (1), $\alpha\mathcal{D}$ describes the friction of the skyrmion, $\mathcal{D} = \int_V d_{ij}\, \mathrm{d}V$. Here, $d_{ij} = \frac{M_s}{|\gamma|}\frac{\partial \boldsymbol{m}}{\partial x_i} \cdot \frac{\partial \boldsymbol{m}}{\partial x_j}$.

We study the effects of a non-uniform perpendicular magnetic field with a longitudinal direction of a nanowire. We neglect thermal fluctuation. The force is given by

$$\begin{aligned} \boldsymbol{F}_g &= -\int H(r) \cdot \frac{\partial M}{\partial x_i} \mathrm{d}^2 r \\ &= -M_s \int H(r) \cdot \frac{\partial n}{\partial x_i} \mathrm{d}^2 r. \end{aligned} \tag{4}$$

The above equation shows the force attribute to the skyrmion edge where the magnetization is reversed. Because we apply the magnetic field along the z-direction while field gradient is in x-direction, force by magnetic field gradient can be expressed as [41]:

$$\begin{aligned} \left(\boldsymbol{F}_g\left(h_g^z\right)\right)_x &= -M_s h_g^z \int x \cdot \frac{\partial n_z}{\partial x} \mathrm{d}^2 r \\ &= 2\pi M_s h_g^z w^2 \int_0^\infty \frac{2t\, \sinh^2\left(R/w\right)}{\sinh^2\left(R/w\right) + \sinh^2\left(\mathrm{r}/w\right)} \mathrm{d}\left(\mathrm{r}/w\right) \\ &= 2\pi M_s h_g^z w^2 f_z\left(R/w\right), \end{aligned} \tag{5}$$

here, h_g^z is perpendicular magnetic field gradient and $f_z\left(R/w\right)$ is only needed to calculate numerically and its asymptotic form is given by $\left(R/w\right)^2/2 + \pi^2/24$.

Then, we consider the one-dimensional equation of skyrmion motion in equation (1). Using magnetic field gradient force and dissipation above with approximation, we can calculate how the velocity of skyrmion depends on the magnetic field gradient in an analytical form

$$\left(\dot{R}\right)_x = \frac{\left(\boldsymbol{F}_g\right)_x}{\alpha D} \cong \frac{|\gamma|}{\alpha} \frac{h_g^z w^2 \left(R/w\right)^2}{\left(R/w\right) + \frac{q^2}{\left(R/w\right)}}, \tag{6}$$

for $q = \pm 1$ and $R/w \gg 1$, the velocity of a skyrmion is simply calculated by

$$v_x \approx \frac{|\gamma|}{\alpha} h_g^z w R. \tag{7}$$

The value of v_x increases with increasing skyrmion radius. The magnetic field gradient force has a large effect on large skyrmion because of sizable magnetic field differences from the left and right sides of the skyrmion. Surprisingly, the skyrmion velocity is proportional to not only the radius of the skyrmion but also the width of the skyrmion. Therefore, we find the relationship between the skyrmion velocities divided by skyrmion width (v_x/w) and the skyrmion radius as follows:

$$\left(\frac{v_x}{w}\right) \approx \frac{|\gamma|}{\alpha} h_g^z R \tag{8}$$

The skyrmion velocity is related to not only skyrmion radius but also skyrmion width. It is might be hard to determine skyrmion width experimentally. Contrary, it can be determined the skyrmion width thorough equation (8), knowing the skyrmion radius and velocity.

3. Micromagnetic simulations

The micromagnetic simulations were performed by using the MuMax3, which is numerically solved the LLG equation [43]. Here, we consider a nanowire shaped with 1000 nm length, 100 nm width, and 1.2 nm thick. The discretized cell for simulations is set to be $2.0 \times 2.0 \times 1.2$ nm^3, which is smaller than the exchange length (~7.5 nm). The skyrmion has not much to do with the simulation cell size, which again manifests that the system discretization does not affect the skyrmion properties [44]. In the simulation, a magnetic skyrmion is nucleated at the center of the nanowire, as shown in figure 1(a). As an example, here the magnetic parameters are saturation magnetization, $M_s = 560$ kA m^{-1}, exchange stiffness constant, $A_{ex} = 12$ pJ m^{-1}, perpendicular magnetic anisotropy energy $K = 1.1$ MJ m^{-3}, interfacial DM interaction energy density $D = 4.0$ mJ m^{-2} [13]. To characterize the size and the shape of the skyrmion, we take normalized magnetization, n_z ($n_z = \cos\ \Theta$) profiles across the center of skyrmion. It can be rewritten the

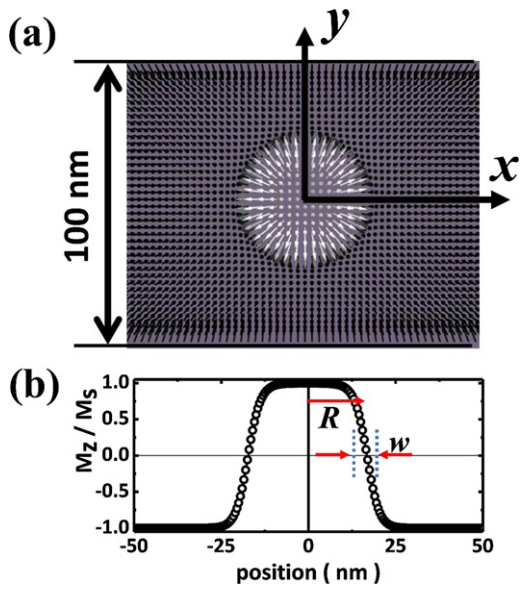

Figure 1. (a) Spin structure of a hedgehog (Néel-type) skyrmion texture in a nanowire film. (b) Line profile across a skyrmion along the longitudinal direction of a nanowire.

Table 1. Magnetic parameters for chosen stable skyrmion. The saturation magnetization of a whole skyrmion is 560 kA m^{-1}.

A_{ex} (pJ m^{-1})	K (MJ m^{-3})	D (mJ m^{-2})	R (nm)	w (nm)
12	1.1	4	22.49	3.57
15	0.7	3	12.82	4.91
15	0.8	3.5	17.18	4.73
15	0.9	4	33.75	4.52
20	1.1	5	24.10	5.77
15	0.4	2	24.10	7.92

line profile across a skyrmion and the skyrmion position along the longitudinal direction of nanowire using equation (3) as

$$n_z = \cos\left(2\ \arctan\left(\frac{\sinh\left(\left(\frac{r-c}{w}\right)\right)}{\left(\sinh\left(\frac{R}{w}\right)\right)}\right)\right), \tag{9}$$

where r is the position of magnetization, c the skyrmion center position, w the width of the skyrmion, and R the radius of skyrmion. The open black circles in figure 1(b) calculated values with the fitting parameter using equation (9). The obtained R and w are 22.49 nm and 3.57 nm, as shown in figure 1(b), respectively. The material parameters in our simulations are chosen as table 1. The magnetic parameters were selected for stable skyrmion conditions. In order to investigate skyrmion motion under applied magnetic field gradient, $h_g^z = (H_{\text{final}} - H_{\text{initial}})/L$, is applied to the whole nanowire along the x-direction. Magnetic field gradient could be generated by a hybrid nanostructure of diluted magnetic semiconductor quantum well [45–47] or using the Oersted field at the edge [48, 49]. Furthermore, using magnetic force microscopy, the radial gradient of the magnetic field [36] can be generated. These gradient fields can drive the skyrmions. We estimated the displacement in terms of the difference between the skyrmion center position at the initial time and at the final time. The initial time is defined at 10 ns after the simulation starts to remove the time period of the transient processes to steady-states [50]. The final time is determined as the moment when the skyrmion reaches the nanowire edge. The skyrmion has a constant velocity during the motion. The skyrmion velocity is obtained from the skyrmion displacement and the time required. Changes of R and w during the motion are less than 5% and 1%, respectively. The contribution of these changes to the velocities is negligible.

4. Magnetic field gradient-driven skyrmions in a nanowire

The skyrmion width and radius are determined by magnetic parameters such as M_s, A_{ex}, K, and D. Since equation (7) implies the skyrmion velocity proportional to the skyrmion radius, however, the skyrmion

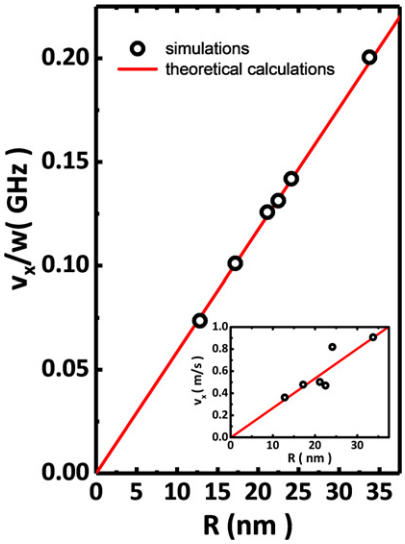

Figure 2. The skyrmion radius dependence of skyrmion velocity divided by skyrmion width (v_s/w) with $\gamma = 176$ GHz T^{-1}, $\alpha = 0.3$, and magnetic field gradient $h_g^z = 1.00$ mT μm^{-1}. The open black circles are micromagnetic simulation results, and red line is theoretical calculation from equation (8). Inset: the skyrmion radius dependence of skyrmion velocity. The open black circles are micromagnetic simulation results, and red line is theoretical calculation from equation (7).

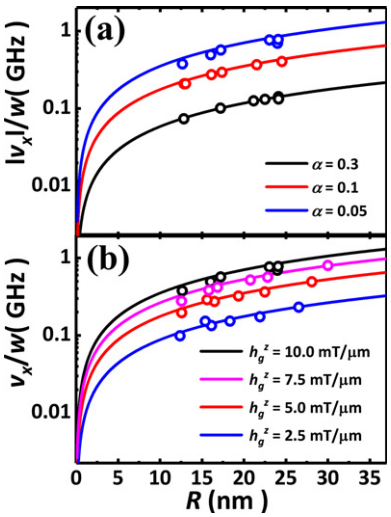

Figure 3. The skyrmion radius dependent of skyrmion motion velocity divided by skyrmion width (v_s/w) on the (a) damping constant, α and (b) magnetic field gradient h_g^z dependence. The open circles are micromagnetic simulation results, and solid lines are theoretical calculation from equation (8).

velocity is not matched well with skyrmion radius as shown in the inset of figure 2. Because the values of skyrmion width are different from each skyrmion, the obtained skyrmion width is from 3.57 to 7.88 nm in the micromagnetic simulation results. The represented skyrmion radius dependence of the skyrmion velocities divided by skyrmion width (v_x/w) is shown in figure 2. The black open circles indicate the simulation result for each skyrmion shown in table 1. The saturation magnetization of a whole skyrmion is 560 kA m^{-1}. The red line is the theoretical calculation with $\gamma = 176$ GHz T^{-1}, $\alpha = 0.3$, and $h_g^z = 10.0$ mT μm^{-1}. The value of v_x/w increase with increasing skyrmion radius. The micromagnetic results are well matched as theoretical expectation results, as shown in equation (8).

Based on the theoretical calculation, other magnetic parameters such as the damping constant and field gradient can also affect the skyrmion motion. In order to reveal the effects of skyrmion motion with various damping constant (α) and field gradient (h_g^z), we perform micromagnetic simulations. Figures 3(a) and (b) indicate the v_x/w with various α and h_g^z, respectively. In figure 3(a) shows simulation results about the damping dependences of the skyrmion v_x/w for the skyrmion radius (open symbols) along with the v_x/w calculated with equation (8) (solid lines). The damping constant varied from 0.3 to 0.05 with $\gamma = 176$ GHz T^{-1}, and $h_g^z = 10.0$ mT μm^{-1}. We find that the v_x/w value increase by decreasing the

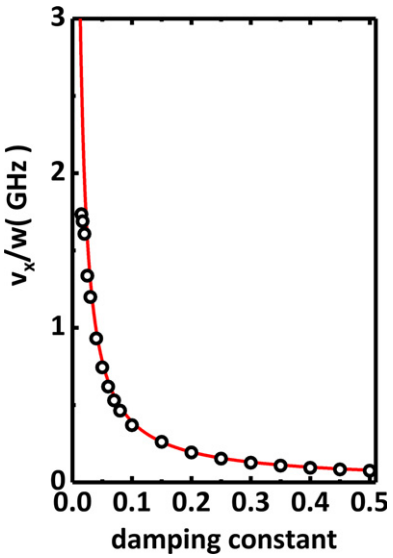

Figure 4. The damping constant, α dependent of skyrmion motion velocity divided by skyrmion width (v_s/w) with $\gamma = 176$ GHz T^{-1}, $R = 23.39$ nm, and magnetic field gradient $h_g^z = 10.0$ mT μm^{-1}. The open black circles are micromagnetic simulation results, and red line is theoretical calculation from equation (8).

damping constant. The v_x/w for various h_g^z obtained by micromagnetic simulations (open symbols) and calculated by equation (8) (solid lines) as a function of skyrmion radius are displayed in figure 3(b). The field gradient varied from 10. 0 to 2.5 mT μm^{-1} with $\gamma = 176$ GHz T^{-1}, $\alpha = 0.05$. As the field gradient decrease, the value of v_x/w decreases. The agreements between the results of micromagnetic simulation and equation (8) are excellent.

In figure 4, we have plotted the v_x/w as a function of α. Magnetic field gradient-driven skyrmions dependence on the damping parameter is investigated at $h_g^z = 10.0$ mT μm^{-1} and skyrmion radius, $R = 22.49$ nm. Here the magnetic parameters are $M_s = 560$ kA m^{-1}, $A_{ex} = 12$ pJ m^{-1}, $K = 1.1$ MJ m^{-3}, and $D = 4.0$ mJ m^{-2}. The black open circles are micromagnetic simulation results, and the solid red line is calculated values using equation (8). The results show the inverse proportionality between v_x/w and α which is consistent with equation (8). We find that the decrease in alpha from 0.5 to 0.0125 increased in v_x/w from 0.07 to 1.79 GHz. The micromagnetic simulation results are in good agreement with the theoretical calculations. Whereas the small damping region, the results from micromagnetic simulations are less than the theoretical calculations. For the damping constant less than 0.02, the terminal time of skyrmion at the edge of the nanowire is incapable since there is not clear to determine the skyrmion velocities. The chiral DW has existed with smaller interfacial Dzyaloshinskii-Moriya interaction energy density cases. We also observe the chiral DW motion in comparison, see appendix A.

5. Numerically calculation on the skyrmion velocity driven by the magnetic-field gradient for small R/w

The analytical formula of gradient field-driven skyrmion motion is presented so far. From micromagnetic simulations and analytic formula, equation (8). We found v_x/w proportional to R in the condition of $R/w >> 1$. The analytic formula for the magnetic bubble dynamics has been reported and Malozemoff and Slonczewski [51] show the velocity of magnetic bubbles with Bloch lines under the external magnetic field in z-direction and its gradient is in x-direction. Without dipole interaction and in the limit of $R/w >> 1$, they obtain the identical equation to equation (6) which approximates equation (4). We also found the velocity of skyrmions along the z-direction magnetic field gradient identical between Bloch and Neel skyrmions. However, under the x- and y-direction magnetic field gradient, skyrmion velocities depend on the skyrmion number and helicities. We recall that our approximated analytical form on the velocity attribute to the approximation for the dissipation dyadic [52]. Although the approximated dissipation dyadic deviates from the real values when $R/w < 3$, only small deviations are introduced in resulting velocities given by equations (4) and (6). In this session, we numerically integrate equation (4) and obtain exact skyrmion motion. Figure 5 shows the numerically and approximately calculated v_x/w^2 with respect to the ratio of R/w comparing to micromagnetic simulation results. Micromagnetic simulations are performed at $h_g^z = 2.5$ mT μm^{-1} and $\alpha = 0.05$. The calculation results cannot be normalized by velocity only since the

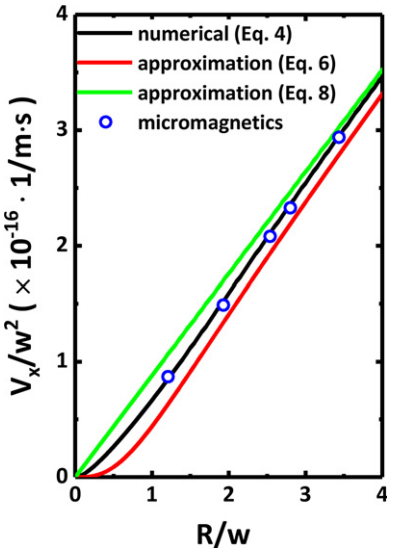

Figure 5. Theoretical calculation of V_x/w^2 versus R/w. The black line is the theoretical calculation from equation (4). The red line is the theoretical calculation from equation (6). The green line is the calculation from equation (8). The open blue circles are micromagnetic simulation results.

simulated skyrmions have different widths. We investigated two more skyrmions for the small R/w ratio. The material parameters for additional skyrmions are summarized as follow: skyrmion (i) $A_{ex} = 25$ pJ m^{-1}, $K = 0.4$ MJ m^{-3}, and $D = 1.9$ mJ m^{-2}, skyrmion (ii) $A_{ex} = 33$ pJ m^{-1}, $K = 0.4$ MJ m^{-3}, and $D = 2.7$ mJ m^{-2}. The ratio of R/w is 1.21 (1.93) for skyrmion (i) (skyrmion (ii)), respectively. The solid black line is a numerical calculation based on the equation (4), the solid red line is an approximated calculation based on the equation (6). The solid green is an approximated calculation based on the equation (8). And the blue open circles are micromagnetic simulation results. For a whole range of the R/w ratio, the micromagnetic simulations agree only with the numerical calculation (solid black line). The spintronics application in which we interested in small size skyrmions requires numerical verification for a detailed analysis.

6. Summary

In summary, we have investigated the skyrmion motion forced by a magnetic field gradient. The velocity of a skyrmion is predicted analytically through the Thiele approach, which agrees well with micromagnetic simulation results for large skyrmions. The skyrmion motion is related to skyrmion shape, Gilbert damping, magnetic field gradient. Interestingly, skyrmion velocities divided by skyrmion width is proportional to the skyrmion radius, magnetic field gradient, and inverse Gilbert damping constant. The numerical calculation results are entirely in agreement with the whole skyrmion size with those of micromagnetic simulation.

Acknowledgments

This work was supported by the DGIST R & D Program of the Ministry of Science, ICT and Future Planning of Korea (20-ET-07), and the Ministry of Internal Affairs and Communications of Japan. J C was supported by the Postdoctoral Fellowship for Foreign Researchers program (No. P16362) of the Japan Society for the Promotion of Science (JSPS).

Appendix A. Magnetic field gradient-driven domain wall dynamics with smaller iDMI energy density

For the cases of the smaller iDMI energy densities, D, chiral magnetic DWs can be formed and the DW energy density is shown as [4, 53]:

$$\sigma = 4\sqrt{A_{ex}K} - \pi D. \tag{A1}$$

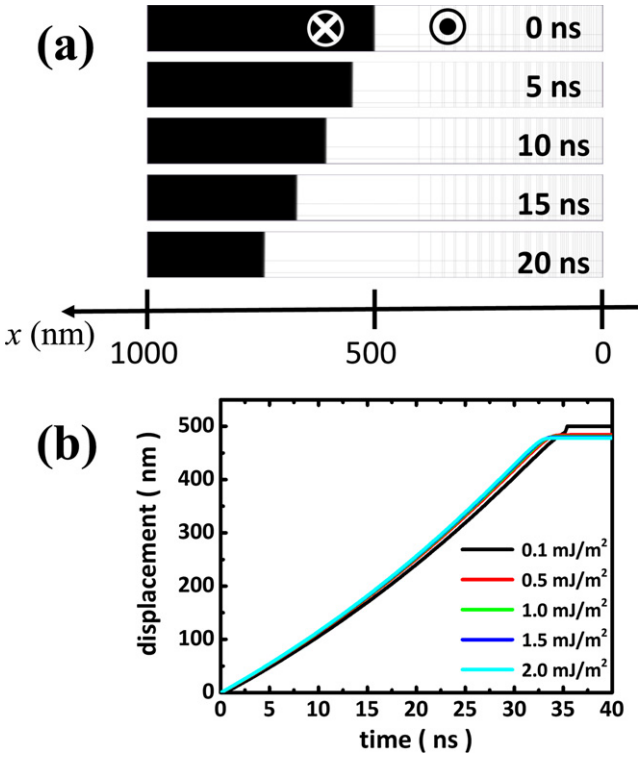

Figure 6. (a) The snapshots of the magnetization at various times. (b) DW displacements as a function of time with various iDMI energy densities. All lines are the DW displacements analyzed by M_z/M_s values.

We now discuss magnetic field gradient driven chiral DW motions. First, the DWs are nucleated at the center of the nanowire. The initial spin configuration of the DWs is parallel to the y-direction and the relaxation process longer than 10 ns is performed. The final spin configuration of the DWs is parallel to $+x$-direction, which is the so-called Néel type DWs. To manipulate the chiral DWs, the magnetic field gradient, h_g^z as 10.0 mT μm^{-1} is applied. The D values coincide with the experimentally determined values [3, 4, 9–12]. The snapshots of the magnetizations as a function of simulation time with $M_s = 560$ kA m^{-1}, $A_{ex} = 12$ pJ m^{-1}, $K = 1.1$ MJ m^{-3}, $\alpha = 0.1$, and $D = 0.1$ mJ m^{-2}, are depicted in figure 6(a). Due to the magnetic field gradient, the chiral DWs move along the $+x$-direction. As shown in colored lines in figure 6(b), the DW displacements are increased and these are saturated after $t = 35$ ns for D is 0.1 mJ m^{-2} and $t = 33$ ns for larger than 0.5 mJ m^{-2}. Surprisingly, the domain wall displacements are almost identical for various D and the chiral DW velocities are approximately 14.2 m s^{-1}, which are much faster than the cases of the skyrmion motions stimulated by the magnetic field gradients. The reason is that the efficiency of the magnetic soliton motions is indeed affected by the geometry of the DWs. When a homogeneous magnetic field is applied to the skyrmion on the nanowire, the Zeeman energy is canceled out for one edge and an opposite edge of skyrmion. That is no driven force to skyrmion. However, the x-directional gradient magnetic field applied to the skyrmion, the Zeeman energy is non-zero for both the edge region of the skyrmion. The force by magnetic field gradient conducts skyrmion motion as shown in equation (5). Therefore, the straight-type chiral DWs have faster DW velocities. Compare with other methods (electrical currents or conventional magnetic fields) to manipulate chiral DWs [54–57], the DW tilting angle is almost negligible for the cases of the magnetic field gradient driven DW motions as shown in figure 6(a).

ORCID iDs

Jaehun Cho https://orcid.org/0000-0001-8096-7454
Chun-Yeol You https://orcid.org/0000-0001-9549-8611
June-Seo Kim https://orcid.org/0000-0002-4105-9901
Hikaru Nomura https://orcid.org/0000-0001-6107-0369

References

[1] Skyrme T H R 1962 *Nucl. Phys.* **31** 556
[2] Rössler U K, Bogdanov A N and Pfleiderer C 2006 *Nature* **442** 797
[3] Soong-Geun J, Kim D-H, Yoo S-C, Min B-C, Lee K-J and Choe S-B 2013 *Phys. Rev.* B **88** 214401
[4] Hrabec A, Porter N A, Wells A, Benitez M J, Burnell G, McVitie S, McGrouther D, Moore T A and Marrows C H 2014 *Phys. Rev.* B **90** 020402(R)
[5] Pizzini S *et al* 2014 *Phys. Rev. Lett.* **113** 047203
[6] Gong C, N'Diaye A T, Kang S P, Kwon H Y, Won C, Wu Y, Qiu Z Q and Schmid A K 2015 *Nat. Commun.* **6** 6598
[7] Yoshimura Y *et al* 2016 *Nat. Phys.* **12** 157
[8] Fert A, Cros V and Sampaio J 2013 *Nat. Nanotechnol.* **8** 152
[9] Cho J *et al* 2015 *Nat. Commun.* **6** 7635
[10] Kim N-H, Han D-S, Jung J, Cho J, Kim J-S, Swagten H J M and You C-Y 2015 *Appl. Phys. Lett.* **107** 142408
[11] Belmeguenai M, Adam J-P, Roussigné Y, Eimer S, Devolder T, Kim J-V, Cherif S M, Stashkevich A and Thiaville A 2015 *Phys. Rev.* B **91** 180405(R)
[12] Nembach H T, Shaw J M, Weiler M, Jué E and Silva T J 2015 *Nat. Phys.* **11** 825
[13] Sampaio J, Cros V, Rohart S, Thiaville A and Fert A 2013 *Nat. Nanotechnol.* **8** 839
[14] Zhang X, Ezawa M and Zhou Y 2015 *Sci. Rep.* **5** 9400
[15] Jonietz F *et al* 2010 *Science* **330** 1648
[16] Yu X Z, Kanazawa N, Zhang W Z, Nagai T, Hara T, Kimoto K, Matsui Y, Onose Y and Tokura Y 2012 *Nat. Commun.* **3** 988
[17] Jiang W *et al* 2015 *Science* **349** 283
[18] Woo S *et al* 2016 *Nat. Mater.* **15** 501
[19] You C-Y, Sung I M and Joe B-K 2006 *Appl. Phys. Lett.* **89** 222513
[20] You C-Y and Ha S-S 2007 *Appl. Phys. Lett.* **91** 022507
[21] Ang C C I, Gan W and Lew W S 2019 *New J. Phys.* **21** 043006
[22] Liu Y-H, Li Y-Q and Hoon Han J 2013 *Phys. Rev.* B **87** 100402
[23] Upadhyaya P, Yu G, Amiri P K and Wang K L 2015 *Phys. Rev.* B **92** 134411
[24] Everschor K, Garst M, Binz B, Jonietz F, Mühlbauer S, Pfleiderer C and Rosch A 2012 *Phys. Rev.* B **86** 054432
[25] Kong L and Zang J 2013 *Phys. Rev. Lett.* **111** 067203
[26] Koshibae W and Nagaosa N 2014 *Nat. Commun.* **5** 5148
[27] Zhang X, Ezawa M, Xiao D, Zhao G P, Liu Y and Zhou Y 2015 *Nanotechnology* **26** 225701
[28] Schütte C, Iwasaki J, Rosch A and Nagaosa N 2014 *Phys. Rev.* B **90** 174434
[29] Oh Y-T, Lee H, Park J-H and Han J H 2015 *Phys. Rev.* B **91** 104435
[30] Jibiki Y *et al* 2020 *Appl. Phys. Lett.* **117** 082402
[31] Nozaki T, Jibiki Y, Goto M, Tamura E, Nozaki T, Kubota H, Fukushima A, Yuasa S and Suzuki Y 2019 *Appl. Phys. Lett.* **114** 012402
[32] Zhang S L, Wang W W, Burn D M, Peng H, Berger H, Bauer A, Pfleiderer C, van der Laan G and Hesjedal T 2018 *Nat. Commun.* **9** 2115
[33] Casiraghi A, Corte-León H, Vafaee M, Garcia-Sanchez F, Durin G, Pasquale M, Jakob G, Kläui M and Kazakova O 2019 *Commun. Phys.* **2** 145
[34] Liang J J, Yu J H, Chen J, Qin M H, Zeng M, Lu X B, Gao X S and Liu J M 2018 *New J. Phys.* **20** 053037
[35] Komineas S and Papanicolaou N 2015 *Phys. Rev.* B **92** 064412
[36] Wang C, Xiao D, Chen X, Zhou Y and Liu Y 2017 *New J. Phys.* **19** 083008
[37] Parkin S S P, Hayashi M and Thomas L 2008 *Science* **320** 190–4
[38] Tomasello R, Martinez E, Zivieri R, Torres L, Carpentieri M and Finocchio G 2015 *Sci. Rep.* **4** 6784
[39] Thiele A A 1973 *Phys. Rev. Lett.* **30** 230
[40] Nagaosa N and Tokura Y 2013 *Nat. Nanotechnol.* **8** 899–911
[41] Wang X S, Yuan H Y and Wang X R 2018 *Commun. Phys.* **1** 31
[42] Braun H-B 1994 *Phys. Rev.* B **50** 16485
[43] Vansteenkiste A, Leliaert J, Dvornik M, Helsen M, Garcia-Sanchez F and Van Waeyenberge B 2014 *AIP Adv.* **4** 107133
[44] Song M, Moon K-W, Yang S, Hwang C and Kim K-J 2020 *Appl. Phys. Express* **13** 063002
[45] Kossut J *et al* 2001 *Appl. Phys. Lett.* **79** 1789
[46] Murayama A and Sakuma M 2006 *Appl. Phys. Lett.* **88** 122504
[47] Halm S, Hohage P E, Nannen J, Bacher G, Puls J and Henneberger F 2008 *Phys. Rev.* B **77** 121303(R)
[48] Kim W-Y and Lee K-J 2013 *Curr. Appl. Phys.* **13** 890
[49] Giordano A, Carpentieri M, Laudani A, Gubbiotti G, Azzerboni B and Finocchio G 2014 *Appl. Phys. Lett.* **105** 042412
[50] Komineas S and Papanicolaou N 2015 *Phys. Rev.* B **92** 174405
[51] Malozemoff A P and Slonczewski J C 1979 *Magnetic Domain Walls in Bubble Materials* 1st edn (New York: Academic) ch 6 p 7
[52] Hrabec A *et al* 2017 *Nat. Commun.* **8** 15765
[53] You C-Y and Kim N-H 2015 *Curr. Appl. Phys.* **15** 298–301
[54] Boulle O, Rohart S, Buda-Prejbeanu L D, Jué E, Miron I M, Pizzini S, Vogel J, Gaudin G and Thiaville A 2013 *Phys. Rev. Lett.* **111** 217203
[55] Ryu K-S, Thomas L, Yang S-H and Parkin S 2013 *Nat. Nanotechnol.* **8** 527
[56] Emori S, Bauer U, Ahn S-M, Martinez E and Beach G S D 2013 *Nat. Mater.* **12** 611
[57] Vandermeulen J, Nasseri S A, Van de Wiele B, Durin G, Van Waeyenberge B and Dupré L 2016 *J. Phys. D: Appl. Phys.* **49** 465003